JOURNAL OF GEOPHYSICAL RESEARCH, VOL. 104, NO. B7, PAGES 15,261–15,279, JULY 10, 1999

Modeling weather fronts to improve GPS heights: A new tool for GPS meteorology?

Thierry L.H. Gregorius[1] and Geoffrey Blewitt[2]

Department of Geomatics, University of Newcastle, Newcastle upon Tyne, England

Abstract. The precision of vertical position and atmospheric water vapor content determined by the Global Positioning System (GPS) is limited by errors due to tropospheric delay. One factor is the spatial and temporal variability in tropospheric refractivity caused by passing weather fronts. We can explain some of the temporal characteristics of estimated tropospheric delay in terms of a simple path delay model as a function of frontal parameters. These results suggest that GPS could be used to estimate the geometry and passage time of a frontal zone. We have developed indices which detect tropospheric variability from GPS data alone; the detection rate of fronts with this approach is up to 70%. Once detected, we eliminated days affected by fronts or other tropospheric variability from the time series of station height estimates, resulting in improved long-term repeatability. The additional variance attributable to fronts is estimated to be up to 10 mm^2 at Herstmonceux, England, where fronts occur every 2–3 days. The effect of fronts on the horizontal station component is up to 80% smaller than for the vertical. Studies in the field of GPS meteorology may be improved by estimating frontal parameters.

1. Introduction

1.1. Background

The Global Positioning System (GPS) is now being used routinely, worldwide, for the precise determination of geocentric latitude, longitude, and height. Typically, these estimates are produced episodically or on a daily basis and are then subject to time series analysis to search for geophysical signals [*Segall and Davis*, 1997]. Height is particularly rich in signal. On a timescale of a few days, effects such as atmospheric pressure loading have been detected in the height component at the level of a few millimeters [*van Dam et al.*, 1994]. Over timescales of years, the time series (appropriately corrected for smaller timescale signals) can be used to estimate height velocity, which is an important parameter for many geophysical phenomena, including postglacial rebound, subduction and collision zone tectonics, and global change in absolute sea level. Unfortunately, height is also the most sensitive component to systematic effects, due largely to errors in modeling the effect of tropospheric refractivity on the signal delay. Unlike longitude and latitude, the signal always comes from the positive hemisphere for height; therefore any systematic shortening or lengthening of the delay will tend to map more into the height than the horizontal components. High precision GPS software packages account for tropospheric refractivity by estimating a zenith delay parameter, which through a mapping function accounts for the slant depth at arbitrary zenith angles. To account for spatial variations, there have been attempts to model gradient parameters, thus allowing for azimuthal variation in delay [*Bar-Sever et al.*, 1998; *Rothacher et al.*, 1998]. To account for temporal variations, stochastic estimation techniques have been used, ranging in sophistication from Kalman filtering and equivalent approaches [*Tralli and Lichten*, 1990] to simply estimating a new bias approximately every hour.

However, none of the above approaches explicitly account for weather fronts, a meteorological phenomenon which sharply divides air and water vapor of different temperatures and hence different refractivity. Even though a Kalman filter, if properly constrained, should in theory be able to cope with any type of variability, this paper presents evidence suggesting that this is not necessarily the case in practice: Weather fronts move over a fixed point on the Earth over a period of one to several hours, during which time we can expect the integrated refractivity (proportional to the delay) to undergo rapid variation, causing a bias in the estimated station position. Weather fronts were initially studied by *Elgered et al.* [1991] and *Johannson* [1992] using microwave radiometers because they were particularly concerned about the effect on space geodetic measurements. The radiometer data showed that the passage of a front was associated with gradients in radio delay, which in half of the cases was greater than 2 cm hr^{-1} (at zenith). They concluded that none of the correlations with various meteorological parameters could easily be used to make reliable predictions of changes or the size of changes in delay.

Given that water vapor radiometers are expensive and not widely available at GPS stations, it would be useful if the GPS data itself could be used to detect weather fronts. If this were possible, then data spanning weather fronts could be removed from the analysis, thus providing an objective way to remove systematic outliers from the height time series. Apart from the purpose of reducing systematic error, another aim of the work presented here is to assess whether GPS has the capability to estimate geometrical parameters of a front and thus possibly benefit studies of meteorological nature.

[1]Now at Nederlandse Aardolie Maatschappij, Shell International B.V., Assen, Netherlands.

[2]Also at Mackay School of Mines, University of Nevada, Reno, Nevada.

Paper number 1998JB900067.
0148-0227/99/1998JB900067$09.00

1.2. Outline

We begin by developing a simple model of excess tropospheric delay due to the passage of a weather front, parameterized in terms of geometrical properties of the front and the refractivity of each segment. We then use this model to understand the characteristics of tropospheric delay in the presence of a front and attempt to explain observed variation in GPS estimated delay in terms of the model parameters. This study also attempts to quantify the accuracy and reliability of the estimated frontal geometry (although this is hard to achieve due to the lack of upper atmospheric data).

Having gained insight into the effect of weather fronts, we then proceed to develop and test an objective measure (a tropospheric "index"), which can be used to decide objectively whether or not rapid tropospheric variability, such as that caused by a passing front, is affecting the data acquired at Herstmonceux, England, which is subject to frequent fronts and for which we had access to an extensive amount of meteorological (met) data and charts. We then apply candidate indices to a 6-month span of daily GPS data from Herstmonceux as well as 20 additional, globally distributed sites and compare the performance of the different candidates with respect to the reduction in variance they yield by removing days they detected as suffering from too variable a troposphere. Finally, we draw conclusions on the causes of tropospheric variability, discuss why some sites are more likely to benefit from this procedure than others, and highlight the implications of this research for the purposes of GPS surveying and meteorology.

1.3. Note on GPS Data Reduction

Throughout this paper, we have applied the precise point positioning technique developed by *Zumberge et al.* [1997] and implemented in the GIPSY-OASIS II software. This technique requires carrier phase and pseudorange data from a single receiver, holding satellite orbit and clock parameters fixed to positions previously determined by the Jet Propulsion Laboratory (JPL) as part of their International GPS Service (IGS) global network analysis. The parameters are therefore all local to the station: three station coordinates, one station clock bias at every epoch, a carrier phase bias to each satellite observed, and a zenith tropospheric bias at every epoch. Using the Lanyi model to map slant delays to zenith, the zenith tropospheric bias is stochastically estimated as a random walk process, with a level of process noise set by the user [*Tralli and Lichten*, 1990]. Note that in this analysis we applied no model accounting for ocean tide loading (because Herstmonceux, the main site of this study located in southeast England, is affected by anomalous, almost nonexistent ocean loading [e.g., *Baker et al.*, 1995]) or atmospheric pressure loading onto the continental crust. We used an elevation angle cutoff of 10° and an observation interval of 5 min.

Precise point positioning is particularly convenient for testing new analysis procedures, since it only requires data from a single receiver and takes only ~2 min to process a 24 hour span of data. This allowed us to analyze the data many times trying several different strategies. As an example, Figure 1 illustrates the effect of varying the level of random walk process noise on the repeatability of station height estimates. Further into this paper, we show how this effect depends on the presence of a weather front.

2. Weather Fronts: Definition, Classification, and Detection

Although many users of the Global Positioning System have a basic understanding of the atmosphere they may not be familiar with the concept of a weather front. Without using too much meteorological jargon, this section provides a brief introduction to weather fronts. For further details the reader is referred to the standard literature, for example; *Barry and Chorley* [1992] or *Meteorological Office* [1994].

A weather front is the boundary between two air masses which display differences especially in temperature, wind direction, and humidity. Depending on the front's direction of motion it is denoted as either cold or warm. If, for a stationary observer on the Earth's surface, warm air is replaced by cold air, it is defined as a cold front. Conversely, if cold air is succeeded by warm air, the front is denoted as warm. Often a warm front is overtaken from behind by a faster moving cold front, eventually resulting in a more complex, merged front called occlusion (or occluded front) which then slowly dissolves as the differences between the bordering air masses gradually disappear.

For some applications it is convenient to model a front as a two-dimensional boundary surface. In reality, however, it is a

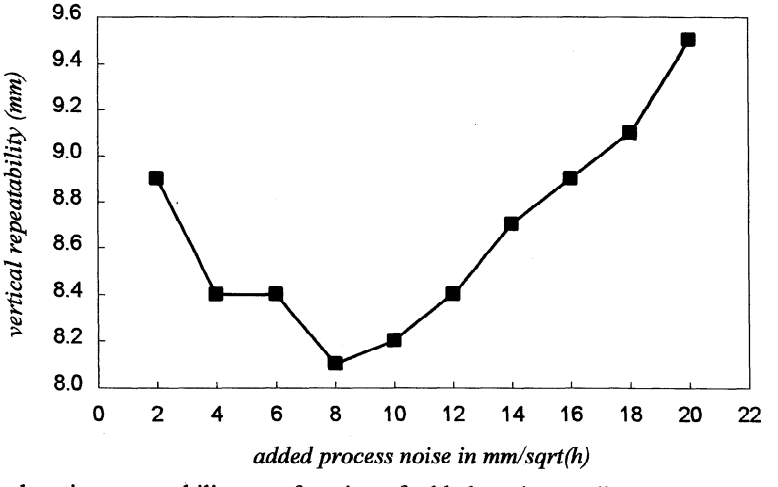

Figure 1. Vertical station repeatability as a function of added random walk process noise. Each point is derived from the analysis of 155 days at Herstmonceux between July 1 and December 31, 1996.

relatively thin, three-dimensional sheet of air that separates the two contrasting air masses. A front is therefore often referred to as a frontal zone and is usually 40–200 km thick. Owing to the clash of different wind patterns, temperatures, and humidities, this zone is subject to rather strong turbulence and cloud formation which then results in precipitation. Near the ground, the evaporation of falling rain in this zone can increase the air's moisture content up to saturation level (100% relative humidity). On a satellite image, fronts can be identified by the long, narrow bands of cloud that accompany them.

The main difference between warm and cold fronts is their inclination. Warm fronts have a very gentle slope, generally not more than 0.5°–1°, and incline toward their direction of movement due to surface friction and the relatively low density of warm air. Cold fronts, however, incline backward because its dense, heavy air subsides and slides underneath the lighter warm air. Near the ground, the cold frontal zone bulges forward because of surface friction. Cold fronts generally have a steeper slope than warm fronts (of the order of 2°).

Because of its gentle slope, the cross section of a front spans many hundreds of kilometers. In practice, the cold, warm, and frontal air layers are stacked on top of each other almost horizontally. For a warm front, upper air clouds associated with the frontal zone can herald the arrival of the front at the ground surface 12 or more hours in advance. It is therefore important to note that common synoptic weather charts always mark the surface fronts, which can lie several hundred kilometers behind (warm front) or ahead (cold front) of the frontal zone at upper levels. The most reliable way of recognizing the passage of a surface front is by changes in temperature, wind, humidity and, sometimes, pressure. On a weather chart, the surface front is often recognizable as a trough of low pressure, causing a kink in the isobars [*Donn*, 1975]. Such a trough may however also be nonfrontal so that fronts cannot simply be inferred by such anomalies in the pressure field [*McIntosh and Thom*, 1969].

3. Modeling GPS Zenith Path Delay Across Weather Fronts

According to J.S. Sawyer in *McIntosh and Thom* [1969], "no idealized frontal model can adequately represent an individual front." Nevertheless, a model can illustrate how much path delay can be expected by a passing front of typical characteristics. We have developed a model to compare the tropospheric zenith path delay expected by the passing of fronts to the delay estimated with GPS at 15-min intervals for Herstmonceux, England. The delay predicted by the model is based on met data recorded on the ground surface.

3.1. Geometric Model Framework

In the absence of upper air met data, which is only available in very low temporal and spatial resolution, our model takes into account three basic sources of input:

1. Recordings of temperature, relative humidity, and pressure on the ground surface.
2. Typical vertical gradients of temperature and humidity for each air mass involved (including those of the frontal zones), which are used to determine the temperature and moisture content in the upper air.
3. The model geometry, including the start time and velocity of the frontal system(s).

The surface data was kindly provided by the Royal Greenwich Observatory which operates the Herstmonceux GPS site. The temperature and moisture vertical gradients of the warm and cold air masses are based on typical upper air values available in the literature (see below), while the vertical gradients in the frontal zones are set to the mean of those of the cold and warm air masses. The remaining parameters, describing the model geometry, are given nominal values and then treated as variables. These parameters are allowed to vary in order to obtain a best fit with the curve of the GPS delay estimates (which serves as "true" reference).

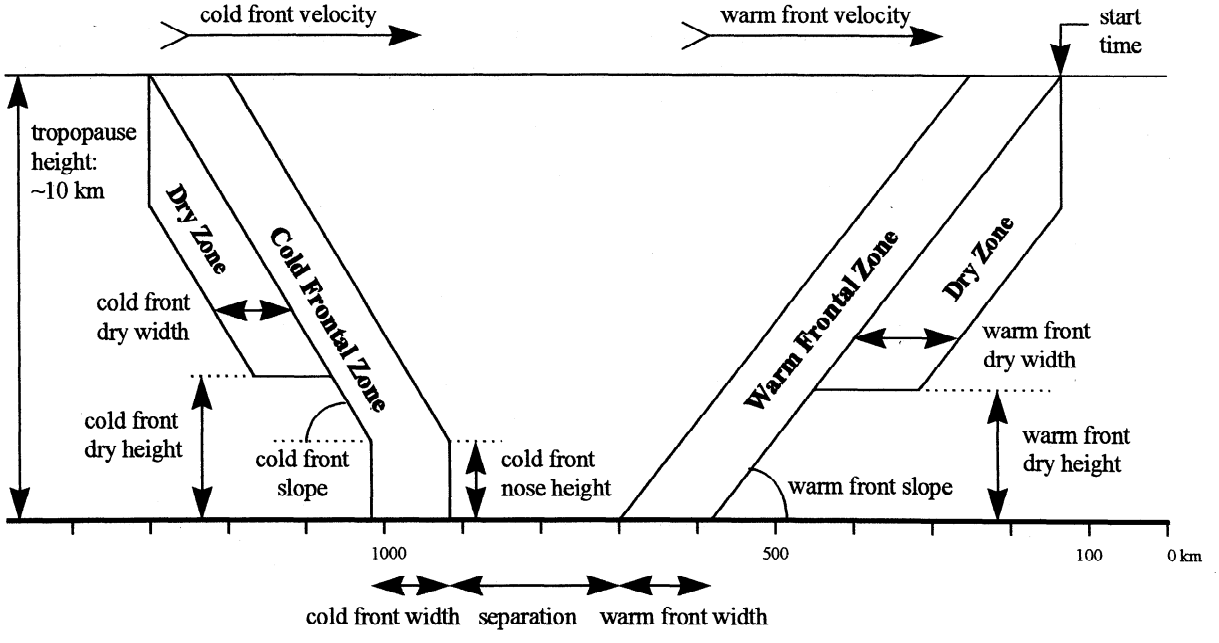

Figure 2. Geometrical model parameters for cold and warm fronts. Note that the model is largely idealized and that in this diagram the vertical scale is greatly exaggerated. A horizontal scale bar is shown to visualize the approximate dimensions of typical weather fronts.

The search for a best fit is carried out with the Downhill Simplex method [*Nelder and Mead*, 1965; *Press et al.*, 1992]. It is essentially a systematic trial and error procedure that can be regarded as an empirical alternative to least squares. The Simplex method is an iterative process designed to minimize a function in a multidimensional parameter space. In our case it minimizes the RMS agreement between the GPS and front model curves of tropospheric delay, which is a function of all frontal parameters shown in Figure 2 (the height of the tropopause was always held fixed to 10 km to reduce the number of parameters).

The parameters are chosen to represent the frontal system shown in Figure 2 with the simplest possible model. Apart from the obvious warm, cold, and frontal air masses there is also a dry zone just below each front [*Meteorological Office*, 1994]. We define the start time of the warm frontal system as the time when the forward edge of the warm frontal zone (at tropopause level) moves overhead the GPS site vertically below. This point is also the origin of our model structure (the abscissa is zero). For the cold front the start time coincides with the arrival of the surface front at the ground station, due to its opposite inclination. Before we can work out the delay for each data point in the met data series, the nature of the air mass(es) overhead must be determined. By multiplying the elapsed time (i.e., the interval between the model start time, as shown in Figure 2, and the actual time of the observation) by the system velocity, the abscissa of the data point in the model structure can be worked out, which then unambiguously defines what type of air mass(es) is (are) present above the site at a given time (in Figure 2, the x axis runs from the right to the left).

3.2. Delay Model

Anywhere in the troposphere, the refractivity, N, can be expressed as a function of temperature, T, total pressure, P, and partial water vapor pressure, e, at that point:

$$N = K_1 \frac{P}{T} + \left[(K_2 - K_1)T + K_3 \right] \frac{e}{T^2} \tag{1}$$

Equation (1) is known as the Smith-Weintraub equation [after *Smith and Weintraub*, 1953], where K_1 (= 77.61 K mbar^{-1}), K_2 (= 72 K mbar^{-1}), and K_3 (= 3.75×10^5 K^2 mbar^{-1}) are the refractivity constants. The units of T and P are degrees Kelvin and millibar, respectively. The zenith path delay, d_{zenith}, incurred by a vertical air column of depth $(h_2 - h_1)$ is obtained simply by integrating the refractive index, n, which can be expressed as a function of refractivity, N, over $(h_2 - h_1)$:

$$d_{\text{zenith}} = \int_{h_1}^{h_2} \left[n(h) - 1 \right] dh = 10^{-6} \int_{h_1}^{h_2} N(h) dh \tag{2}$$

N can be numerically integrated as a function of elevation, h, because temperature, pressure, and vapor pressure all vary (generally decrease) with height above the ground. Where the vertical column above the GPS site contains different air masses stacked on top of each other, the delay incurred by the thickness of the troposphere is obtained by integrating equation (1) individually over the depth of each layer and then adding up those partial delays. Also, by integrating the first and second term of this equation separately, the "dry" and "wet" contribution to the delay can be determined independently.

3.3. Implementing the Delay Model in the Geometric Framework

We make the assumption that throughout the troposphere temperature and water vapor concentration decrease (near) linearly with height, as suggested by the near-linear standard lapse rates given by *Barry and Chorley* [1992, Tables 4.1 and 4.2], for example. We therefore ignore possible temperature inversions, which can happen near the ground surface at night, and other possible nonlinear deviations: These should only have a very small effect on the total delay. To model meteorological conditions in the upper air, we thus apply the following vertical gradients to the surface data:

1. Warm air: temperature –5.1 °K km^{-1}, humidity mixing ratio –1.02 g kg^{-1} km^{-1}.
2. Cold air: temperature –6.4 °K km^{-1}, humidity mixing ratio –0.95 g kg^{-1} km^{-1}.
3. Warm frontal zone: temperature –2.9 °K km^{-1}, humidity mixing ratio: –0.98 g kg^{-1} km^{-1}.
4. Cold frontal zone: temperature –2.9 °K km^{-1}, humidity mixing ratio: –0.98 g kg^{-1} km^{-1}.
5. Warm frontal dry zone: temperature same as for cold air, humidity not applicable (= 0).
6. Cold frontal dry zone: temperature same as for cold air, humidity not applicable (= 0).

The humidity mixing ratio is in grams of water vapor per kilogram of dry air. The dry zones are modeled to have no water vapor at all. The warm and cold air gradients are based on typical upper air values of maritime tropical and maritime polar air, respectively. The frontal zones are modeled with the mean of the cold and warm air mass gradients. The variation of pressure with height is given by the relationship

$$dh = -(RT / gP) dP \tag{3}$$

where R is the universal gas constant and g is the gravitational acceleration [*Meteorological Office*, 1994].

We apply the following procedure to model upper air data. The surface met data provides the temperature, pressure and water vapor density to determine the refractivity at the bottom of the air mass. Readings of relative humidity are easily converted into water vapor density using pressure and temperature together with tabulated values of saturation vapor pressure versus temperature (which are widely available in the literature [e.g., *McIntosh and Thom*, 1969]). The temperature and water vapor gradients specified for that air mass are then used to extrapolate the temperature and moisture levels throughout that layer while pressure is determined with equation (3), which enables us to derive the delay inferred by each air mass under consideration. If, along the vertical column cutting through the troposphere, there is any air mass present in upper levels that is different from the one touching the ground, then temperature, pressure, and water vapor content throughout that upper air layer are derived by applying its typical gradients to the mean of all surface met data points recorded at the time when this air mass touches the ground. For example, to model the conditions in a frontal zone present in the upper air, the frontal gradients are applied to the mean of all data points recorded on the ground during the passing of the surface front. Because we also model atmospheric pressure in this manner, this would, strictly speaking, violate the hydrostatic equation if there are pressure changes over time. However, this equation implies that the atmosphere is one relatively homogeneous block of air. Since the borders be-

tween different air masses are subject to strong turbulence, there can be rapid pressure jumps at altitude in the frontal zones.

With the model presented here, we try to obtain a more appropriate representation of such dynamics by modeling the properties of each air mass separately. We assume that each air mass is in hydrostatic equilibrium within itself, but we allow this balance to break down along air mass boundaries. For the main purpose of this analysis, i.e., to illustrate how weather fronts can cause rapid variations in delay, this simplification should be sufficient, and it is also more intuitive than using tools from fluid mechanics or other theories to model the complex dynamics of the atmosphere.

What we term "tropospheric" delay actually also includes the delay incurred by the stratosphere (which is of the order of ~0.5 m). We assume that the stratospheric contribution to the delay is entirely dry and thus only apply the first term of the Smith-Weintraub equation. The stratospheric temperature gradients employed are those of the 1976 U.S. Standard Atmosphere. Since we have no other met information than readings taken on the ground surface, we first smooth the extrapolated refractivity values at tropopause level with a large moving average window (24 hours) before integrating the delay through the different stratospheric layers. We found that with a window of 24 hours we get the best agreement of the predicted total delay with the GPS estimates of delay. Using a window shorter than 22 or longer than 24 hours produced worse RMS agreements. Intuitively, it also makes sense that stratospheric temperature and pressure are related to the troposphere below; only that in the stratosphere, any changes occur more gradually than at lower atmospheric layers, explaining the requirement of a large smoothing window. Using no smoothing window at all produced the worse results (irrespective of whether or not separate gradients were used for each air mass).

3.4. Model Limitations

In practice, the transitions from one zone to another are more gradual than we assume here. Introducing those sharp boundaries of temperature and moisture inevitably leads to (usually minor) step functions in the modeled delay time series.

Also, with linear vertical moisture gradients, the modeled water vapor content is zero beyond a certain elevation (typically ~4–5 km, depending on the level of surface moisture). That is, we ignore any water vapor that is present above that ceiling. This is not a problem in practice since the moisture content in the upper tropospheric layer is very small and distributed relatively homogeneously, which should merely introduce a very small, constant offset to the modeled wet delay. (Also, the dry zones are actually smaller than indicated in Figure 2; they do not generally extend to the tropopause. Because of the relatively low water vapor ceiling, however, this simplification does not make any difference in practice.) Clearly, when ground-based measurements of water vapor are not representative of the state of the troposphere aloft, this will limit the model's ability to accurately determine zenith delay. With the absence of upper air data, there is however no other option than to use ground observations. In practical terms, we can thus only test the model on data for which there is a high correlation between surface humidity and wet zenith delay.

Another requirement related to the lack of upper air data is that the standard gradients used must actually represent the physical properties of the air masses modeled. If this is not the case, this will obviously limit the model's performance, and the predicted delay will end up having a near-constant offset to the true delay.

Then, increased refractivity due to cloud and precipitation as well as the bending of the path are ignored, although a certain amount of additional moisture within the frontal zones could in theory be simulated by reducing the frontal moisture gradients (which effectively raises the water vapor ceiling and thus increases the wet contribution to the delay). Finally, we generally assume that it is valid to compare the model with zenith delays estimated with GPS, where no account has been taken for gradients in the mapping function. This assumption is based on the very shallow front slopes, considering that the fronts are an order of magnitude broader than the height of the tropopause. However, as we discuss later, we expect this to cause larger errors in height estimation.

3.5. Model Performance

We tested our model on a selection of frontal days, for which the best fit with the GPS estimates was obtained. Here, we shall only present one example: a warm front, followed by a cold front, on November 29, 1996. This example meets the two main model requirements: (1) the correlation between surface absolute humidity and estimated wet zenith delay is high (0.92) and (2) the standard gradients appear to describe the air masses involved rather accurately since the agreement of the model-predicted and GPS-estimated tropospheric delay is to within a few millimeters, especially before and after the passage of the fronts (Figure 3).

For this analysis, we considered the 72-hour time series from 0000 LT on November 28 to 2400 LT on November 30. Except for the velocities, for which we had rough estimates from the weather charts, we applied relatively loose constraints to the parameters in order not to bias the results by a preconceived "educated guess." We thus constrained the Downhill Simplex algorithm to estimate the model parameters within the following boundaries (applied similarly to cold and warm fronts, except as noted):

system start time	1–50 hr
separation	40–400 km
velocity (warm)	38–48 km hr^{-1}
velocity (cold)	38–63 km hr^{-1}
slope	0.3–1.5°
width	20–220 km
dry width	10–200 km
dry height	2–6 km
nose height (cold)	0.5–3.5 km

In addition, the velocity of the cold front was constrained to be greater than that for the warm front.

Specifying a tolerance of 10^{-5} for the size of the simplex as termination criterion [see *Press et al.*, 1992], the Downhill Simplex routine required 318 model evaluations to derive the solution shown in Figure 3. The RMS agreement with the GPS estimates of tropospheric delay is 6.2 mm over the 72 hours; the difference at each point never exceeds 2 cm. The uniform model shown represents a homogeneous, idealized atmosphere with no frontal structures. It is derived by applying equations (1), (2), and (3) to every surface met data point while using the mean temperature and water vapor gradients of the warm and cold air masses (the refractivity values at the tropopause are smoothed in the same way as for the front model). For this model, the RMS agreement is 11.6 mm, with

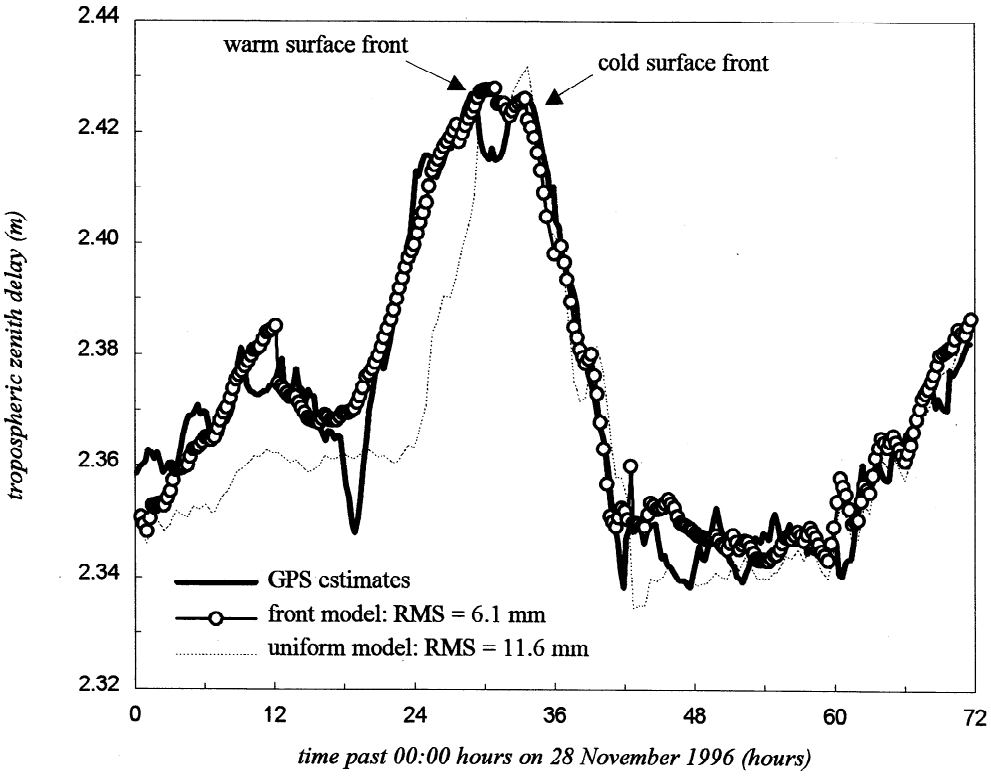

Figure 3. Model-predicted and GPS-estimated zenith path delay at Herstmonceux on November 28–30, 1996. The RMS agreement of the front model with the GPS estimates is 6.1 mm. In comparison, the uniform model only agrees to 11.6 mm RMS.

differences up to 4 cm during the approach of the warm front. The front model therefore improves the agreement with GPS-estimated delay, with a square root variance reduction of 9.8 mm. This does not in itself prove model fidelity, but it does demonstrate that the front model can satisfactorily accommodate the obvious discrepancy between the uniform model and GPS-estimated delay shown in Figure 3. Because of the high correlation between surface and upper humidity, the agreement of the uniform model is also fairly good but deviates considerably from the "true" delay particularly during the approach of the warm front (as described later in this section).

In this example, the model therefore fitted the GPS data extremely well. The parameters were estimated as follows:

system start time	9.3 hr
separation	122.5 km
velocity (warm)	42.3 km hr^{-1}
velocity (cold)	48.8 km hr^{-1}
slope (warm)	0.73°
slope (cold)	1.29°
width (warm)	127.0 km
width (cold)	142.1 km
dry width (warm)	20.9 km
dry width (cold)	79.1 km
dry height (warm)	3.7 km
dry height (cold)	3.4 km
nose height (cold)	0.6 km

Owing to the lack of upper atmospheric sounding data we do not know their true values, but at first sight the Simplex-derived estimates seem reasonable, especially the slope of the frontal zones: The cold front slope came out steeper than the warm front slope. The most reliable indicators of the parameter accuracy are the estimated times during which the surface fronts passed the site. These can be derived directly from the start time, velocity and frontal geometry parameters. On a weather chart, fronts are marked by lines which roughly indicate the center of the frontal zone on the ground surface. Our model estimated that the warm surface front passed over the site during the period of 27.8–30.8 hours. On the weather charts used by the Meteorological Office, the frontal line crosses the station at about 0600 LT on November 29, that is, at 30.0 hours, which is within the bounds predicted by the model. Similarly, the surface cold front is computed to be present between 33.7 and 36.6 hours: The weather charts state 1030 LT, i.e., 34.5 hours, which is again within the estimated period. Our model has thus correctly predicted the passage times of the fronts, which indicates that the above parameters must be reasonably accurate.

To get an estimate of the individual parameter uncertainties, we had to perform a simplistic trial-and-error approach because the Downhill Simplex algorithm does not incorporate a stochastic model (unlike least squares). We therefore took the optimum parameter estimates and changed them, one by one, to see how each of them affected the outcome of the final RMS agreement. If a small change resulted in a large increase of the RMS, then it could be accepted that the parameter had a small "formal" error. We found that this was the case for the inclination and the start time of the fronts. Despite the loose constraints, the RMS worsens by 50% when changing the start time by just 4.2 hours. Similarly, the inclination of the fronts have an "uncertainty" of ~0.2°. All the remaining parameters, however, can vary within their loosely defined con-

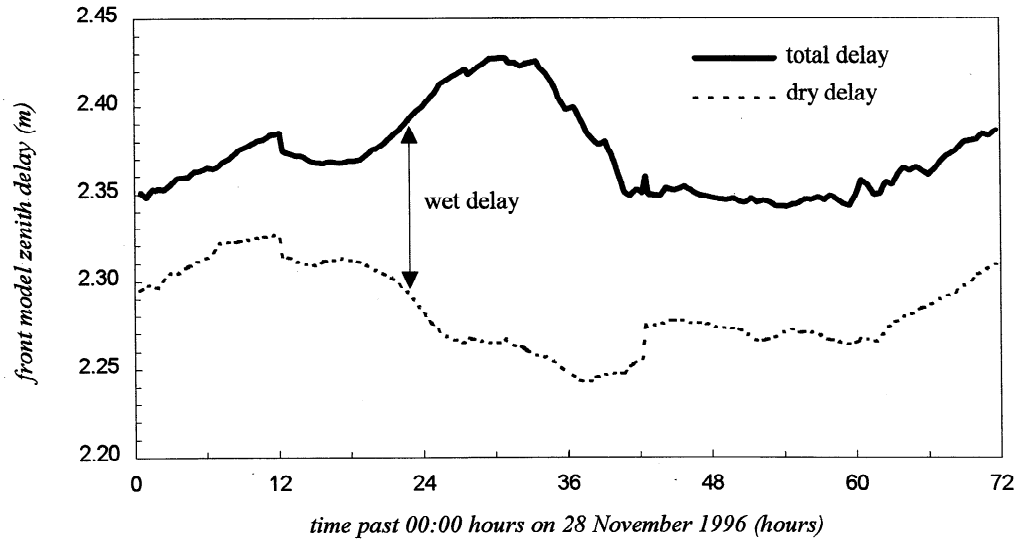

Figure 4. Total and dry delay predicted by the front model; the difference is the wet delay. The wet part of the delay temporarily increases during the approach and passage of the warm and cold fronts, which is from ~24 to 40 hours.

straints without significantly affecting the final solution. This indicates that GPS is able to resolve gradient-related parameters (i.e., the frontal start time and inclination, both also closely related to passage time), which is confirmed by studies such as *Rothacher et al.* [1998], but also that GPS does not have the data strength to sense elaborate structures such as the frontal dry zones or the cold front nose height. We therefore believe that these remaining parameters are therefore also highly correlated with each other.

In all the examples we tested, even those where the two main model requirements were not met (as explained above), the inclination of the cold front always came out steeper than that of the warm front, thereby confirming frontal theories. In our 6-month data set we only had two instances where the model requirements were more or less fulfilled during the passage of fronts (including the example presented here). In the other test, the estimated passage times agreed to within ~1 hour with the information provided by the weather charts. Considering that the frontal lines on these maps are drawn freehand, and often in a hurry (Mick Wood, U.K. Meteorological Office, private communication, 1997), this is well within an acceptable error margin. We also tested the front model on data acquired at Delft, Netherlands, for the same time span. The warm and cold fronts which passed Herstmonceux from the northwest on November 29 moved over Delft, located roughly 350 km to the northeast, ~2 hours later. Despite a very low correlation between surface humidity and wet zenith delay at Delft (<0.30), the model correctly estimated that the separation of the two fronts had become narrower than at Herstmonceux (97.8 km compared to 122.5 km), the magnitude of which was confirmed by the weather charts. The inclinations of the warm and cold fronts at Delft was estimated to be 0.51° and 1.47°, respectively.

Usually, the approach and passage of fronts temporarily increases the amount of water vapor present in the troposphere and thus the wet delay. This is well illustrated by Figure 4, which depicts the dry and wet parts of the delay estimated by our model. Interestingly, when comparing the front model with the uniform model, also the dry part of the delay is affected. This is caused by the (relatively rapid) variations in temperature which originate from the contrast of the two air masses on either side of a front. These changes affect atmospheric pressure and especially the dry delay which is a function of temperature and pressure, as seen in equation (1). The difference between the dry frontal and uniform models is illustrated in Figure 5a; at some points it reaches almost 2 cm. Unfortunately, the front model delay is plagued by step functions due to the limitations discussed above. Although a small part of these jumps (~20%) are due to the modeled pressure, the step functions are largely due to discrepancies in temperature which become attenuated at altitude when extrapolating surface temperatures with different gradients for different air masses. The actual changes in delay are therefore likely to be more gradual than those shown in Figure 5a. However, the results still indicate that the difference between the front and uniform model can be significant during the passage of fronts. Using a standard atmosphere to model the dry delay (which is wide practice in the GPS and very long baseline interferometry community) would thus not be appropriate in the presence of fronts.

Figure 5b shows the discrepancy in wet delay between the frontal and uniform models. As could be expected, the differences in this case are greater than for the dry part of the delay: during the approach of the warm front even up to 6 cm. The difference in total delay between the frontal and uniform model, as illustrated in Figure 3, is thus mainly due to the way water vapor is modeled. The uniform model extrapolates each reading of surface moisture (at 15-min intervals) to higher layers vertically above the site in a straightforward way. The front model does the same only if the vertical air column above the ground station is taken up by a single air mass. Where, for example, the warm air mass encroaches over cold air and is thus only present in upper layers of the column, the mean surface humidity of the warm air is extrapolated to its present altitude using the warm water vapor gradient. Since the warm air parcel encroaches over the cold air at both ends,

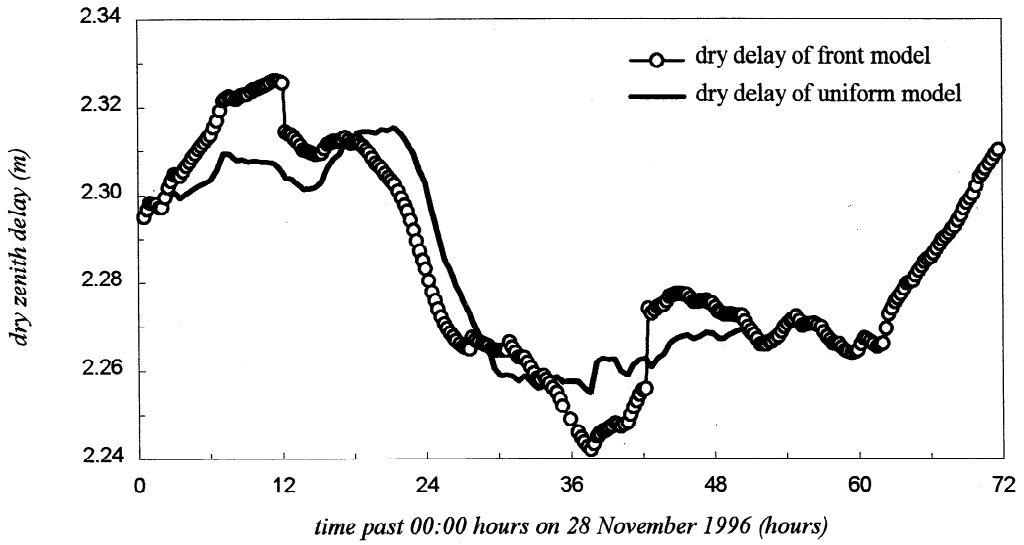

Figure 5a. Difference in dry delay between the frontal and uniform model. The two step functions in the front model are caused by the sharp changes in temperature which become attenuated with altitude due to different temperature gradients being applied to different air masses.

this will significantly change the modeled delay from that of the uniform model which would apply the cold water vapor gradient throughout the entire height of the column (the same applies to the modeling of the frontal zones).

In summary, we have thus been able to explain the variability of the troposphere encountered during the passage of fronts with a simple model. Even though this front model, as it stands, has no immediate use for the purpose of GPS meteorology, a refined version could be incorporated into GPS data reduction software to estimate gradient-related parameters (such as the inclination and passage time) of weather fronts. This analysis suggests that GPS does have the data strength to estimate such frontal parameters with relatively high confidence. Properly implemented, this type of model could have benefits for the study of weather fronts, either for the purpose of operational weather forecasting or fundamental climatic research. Even though the advantages of a front model would probably be limited in regions where dense GPS meteorology networks exist (because these allow the computation of three-dimensional tomographies of the troposphere), the use of GPS for the monitoring of fronts could be useful in isolated areas, such as the mid-oceans, where GPS receivers and meteorological data are scarce. A single receiver, installed on a mid-ocean island, could possibly provide valuable data about the shape and passage times of fronts moving across the region.

4. A Tropospheric Index to Reduce GPS Systematic Error

Weather fronts usually leave a clear signature in the time series of tropospheric delay: They often stand out as peaks (Figure 6). Most models used to date in GPS or very long baseline interferometry analyses to evaluate the effect of the troposphere on signal propagation are based on standard,

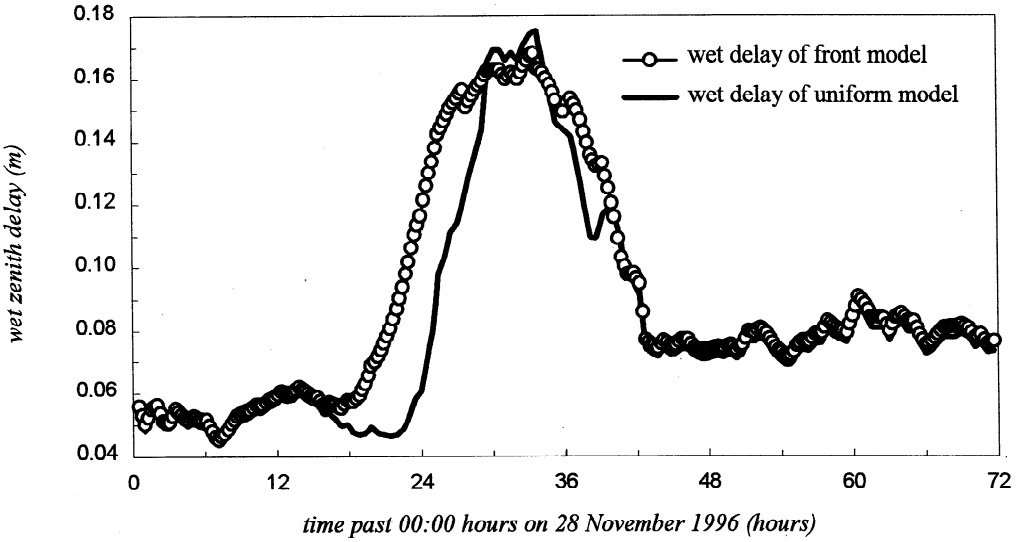

Figure 5b. Difference in wet delay between the frontal and uniform model. There are no step functions here because the modeled water vapor ceiling is quite low and does not extend into the upper troposphere.

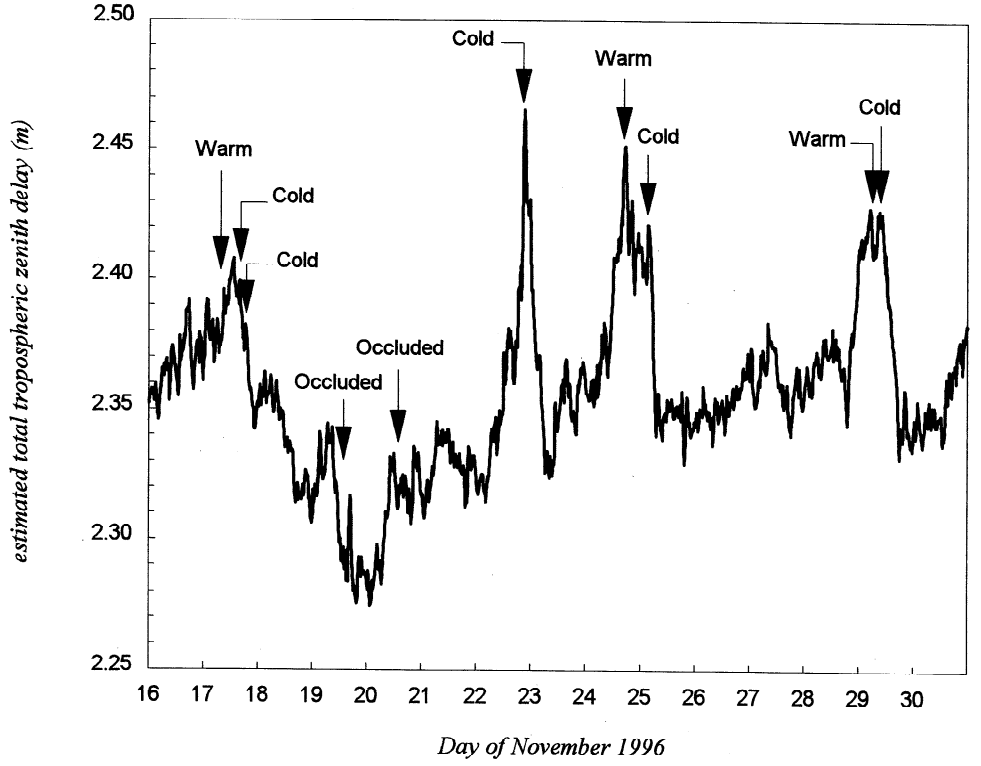

Figure 6. A 15-day time series of total tropospheric zenith delay, as estimated with GPS at Herstmonceux, using a random walk constraint of 15 mm $hr^{-1/2}$. The passage of most surface fronts (marked as warm, cold, or occluded) leaves a clear signature on the delay.

idealized atmospheres that do not account for weather fronts. Fronts do not just incur rapid variations in zenith tropospheric delay, they also affect each satellite-receiver line differently due to their asymmetrical shape. Since inaccuracies in the delay model inevitably bias the GPS estimates of (especially) vertical station position, we now quantify the magnitude of systematic error that can be expected in GPS height time series from the passing of fronts. Later in this paper we will also briefly discuss the effect of weather fronts on the horizontal station component, but, as this is much smaller in magnitude, we focus this investigation on station height. Relying on real-time weather charts obtained from the U.K. Meteorological Office, we first eliminate days that are affected by fronts and note the improvement of vertical repeatability at Herstmonceux, South England. We then develop indices to identify such days from the GPS data alone, without the need to refer to any meteorological data source, and test their performance on Herstmonceux data by checking the overlap of days rejected by these indicators with those days affected by fronts. Such indices are not only useful to detect fronts but, more importantly, to improve the station repeatability by removing data affected by high tropospheric variability in general (which may also arise because of phenomena other than fronts). The ultimate aim of the index analysis is therefore to reduce systematic error with the study of tropospheric variability (regardless of whether or not it is caused by fronts). We also apply the indices to tracking data from 20 globally distributed sites, covering most types of climates, to test the subsequent reduction of variance as a function of latitude or climate (with no meteorological data input).

4.1. Effect of Weather Fronts on Station Height Time Series

To assess the effect of weather fronts on vertical station repeatability at Herstmonceux, we checked the real-time working charts of the U.K. Meteorological Office and labeled all days in the time series according to whether or not they were affected by the passage of one or more surface fronts. Most fronts moving across Great Britain originate from the North Atlantic and arrive about every 2-3 days. Under stormy conditions, there can be as many as 3-4 fronts in 24 hours. Unfortunately, Herstmonceux suffered from a hardware problem that required certain outliers to be deleted from the height time series. It is believed that these may have been caused by poor connectors in the receiver hardware (Philip Gibbs, Royal Greenwich Observatory, personal communication, 1997). To remove bad days we used a data snooping procedure where we rejected all points with a residual-repeatability ratio >3.5 (Figure 7).

Out of the 155 days processed, 57 were affected by cold, warm, or occluded fronts (corresponding to 37% of the entire series). When excluding those frontal days from the time series the repeatability improves considerably, especially if the amount of process noise added to the random walk model is high (Figure 8). Overall, when not rejecting any days from the time series, the repeatability varies by 1.4 mm depending on the level of process noise applied. The best repeatability, 8.1 mm, is obtained with a random walk constraint of 8 mm $hr^{-1/2}$. This is also the level at which the difference in repeatability between days with and without fronts is smallest (0.4 mm), confirming that this must be the optimum strategy. The opti-

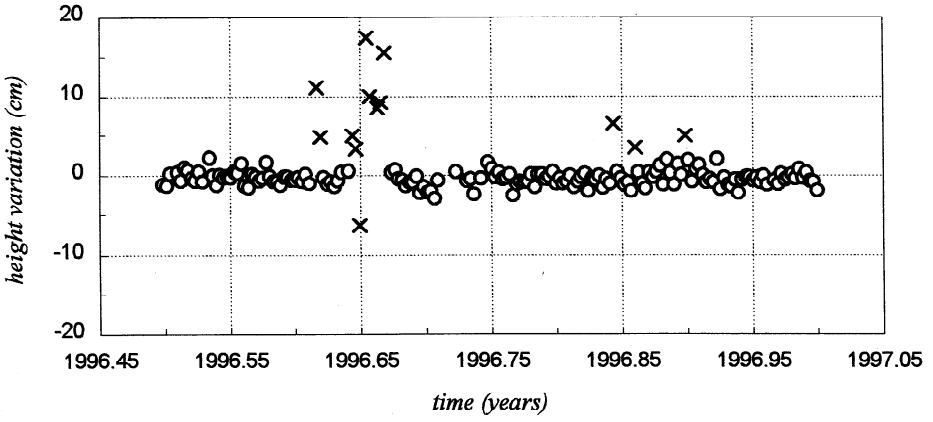

Figure 7. Herstmonceux height time series, illustrating problems due to hardware. If the residual (derived from linear regression) divided by the overall repeatability was >3.5, then the day was rejected as an outlier. From the 168 days, 13 were excluded (marked with a cross), resulting in a 155-point series. The repeatability thus came down from 23 to 8 mm.

mum constraint for Herstmonceux is thus slightly smaller than the value of 12 mm $hr^{-½}$ which *Dixon and Kornreich Wolf* [1990] found to minimize repeatability in Central and South America, but we would expect the optimum value to vary geographically (which is also confirmed by Table 3 later in this paper).

The discrepancy between repeatability on frontal and nonfrontal days grows up to 1.6 mm as soon as one moves away from that minimum. From Figure 8 it is also apparent that days affected by fronts are more sensitive to the choice of constraint in the random walk model for tropospheric delay. While the repeatability of front-free days does not vary by >0.5 mm between the constraints of 2 and 16 mm $hr^{-½}$, the variability of the "frontal" repeatabilities is almost 3 times greater.

The contribution of weather fronts to the variance thus depends on the level of process noise applied. At the optimum constraint of 8 mm $hr^{-½}$, weather fronts only contribute (8.11 mm)^2 − (7.97 mm)^2 = (1.5 mm)^2 to the variance of the full time series, corresponding to 3.4%. The difference in variance between the frontal and nonfrontal days at this level is (2.7 mm)^2. At 2 mm $hr^{-½}$, however, days affected by fronts make up (3.2 mm)^2 = 10 mm^2 of the full variance, corresponding to 13.1%. Here the difference between days with and without fronts is (5.5 mm)^2. (As an aside, it should be mentioned that the detrimental effect of weather fronts on station height becomes much worse when a less optimal processing strategy is used. For example, when estimating tropospheric delay as a constant parameter, as is fairly common practice for commercial-type software packages, the repeatability is 17.2 mm. By

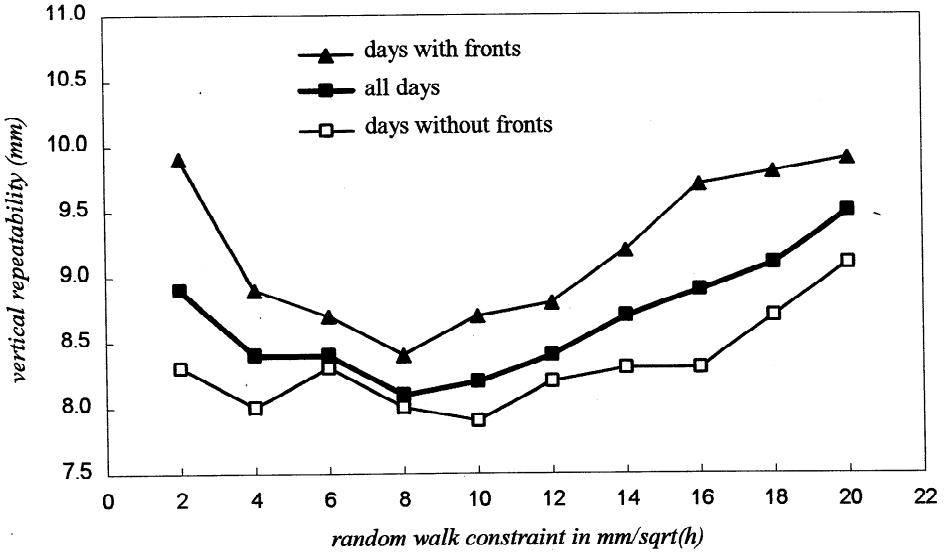

Figure 8. Repeatability as a function of random walk process noise and the passage of weather fronts at Herstmonceux. Days affected by weather fronts are more sensitive to the choice of process noise level. The number of days processed for each time series is 155 for "all days," 57 for "days with fronts" and 98 for "days without fronts."

removing days affected by fronts, the repeatability improves by 2.9 mm. In this case, the difference in repeatability between frontal and nonfrontal days is statistically significant by a large margin: The fronts contribute over 30% to the vertical time series variance).

If we knew the exact beginning and end times of the periods during which weather fronts had a noticeable impact on the estimated tropospheric delay, then their contribution to the variance could be worked out more accurately and would, without a doubt, be higher still than the figures we present here. Classifying a whole day as frontal even if only a few hours were under the influence of a front certainly weakens the results. Unfortunately, we have no objective measure for determining those periods of influence, and if we tried to guess their times by inspecting the plots of estimated tropospheric delay we would introduce a human, subjective bias.

4.2. Fractal and Other Methods to Quantify Tropospheric Variability

As weather fronts produce rapid variations in tropospheric delay, we need an objective method of quantifying such changes to construct a reliable index. We estimated the delay at 15-min intervals, resulting in a discrete time series of 96 points per day. To ensure consistency in the daily comparisons, we only use days with a full 24-hour set of tracking data. For each 24-hour arc we then plot the curve of tropospheric delay versus time and use the following selection of indicators to assess the level of tropospheric variability: (1) The fractal dimension of the curve (FRACT), (2) the length of the curve over the 24-hour period (LOC), and (3) the magnitude of the gradients found along the curve (GRAD). To determine the fractal dimension of the curve, we apply the Mandelbrot-Richardson [e.g., plot *Roach and Fowler*, 1993].

Inspired from the principle of fractal dimension, we also use an even simpler index of variability: the length of the curve over the reference time interval of 24 hr (for practical reasons it is actually 23.75 hr, from 0000 to 2345 LT inclusive; 2400 LT is used as 0000 LT the next day). When plotting time in hours and delay in meters, the unit of curve length would be $\mathrm{sqrt}(\mathrm{hr}^2+\mathrm{m}^2)$. A totally unconventional flat curve would have the shortest possible length of 23.75 units: The longer the curve, the higher the variability of the troposphere.

Finally, we test an indicator based on curve gradients, for which we compute the slope of each curve segment. For each point, we then compute the mean gradient of the 1 hour window (consisting of 5 data points spaced at 15 min intervals) extending from −30 to +30 min. Counting the number of data points that have a greater mean gradient than a certain, predefined threshold, we get an indication of variability. In this analysis we use a 1 cm hr^{-1} threshold because we found that this approach, combined with 1-hour averages, produced the best detection rate of fronts (we tested this with thresholds varying from 1 cm hr^{-1} to 12 cm hr^{-1} and window lengths of 0–3 hours but with 8 mm $\mathrm{hr}^{-1/2}$ of random walk process noise in all cases: with different levels of process noise the optimal GRAD settings are likely to change).

4.3 Index Implementation and Test Description

The indices are implemented to determine the level of tropospheric variability for each day in the time series. Any day that yields a value above a certain cutoff threshold is then flagged as being too variable and excluded from the series. To a certain extent, the vertical repeatability should improve with the number of days rejected.

To assess the ability of an index to detect weather fronts from GPS data alone, we check the overlap of the days rejected using a particular detection method with those affected by fronts. We carry out this part of the analysis with Herstmonceux data only, since this is the only site for which we had full access to meteorological ground observations and weather charts.

We then apply the three indices also to 20 globally distributed sites to investigate their effect on repeatability as a function of climate. We did not obtain any met data for these additional stations. This part of the analysis is therefore limited to the reduction of systematic error based on tropospheric variability in general, not weather fronts in specific (some sites are not likely to be affected by fronts anyway). The selection of stations used is shown in Figure 9.

For each of these stations we processed 6 months of data, from July 1 to December 31, 1996. As mentioned above, only days with a full 24-hour set of data were considered in our analysis. With the exception of Herstmonceux (as described in the section 4.2), no station required outlier removal prior to carrying out the investigation described below.

4.4. Index Performance at Herstmonceux

First, to assess the capability of an index to identify fronts from GPS data alone, we fine-tune the cutoff threshold so that the same number of days as the known number of days affected by fronts is rejected. Next, to establish the optimum number of days to exclude for each station, we use a selection of variability cutoffs fine-tuned to reject 10, 20, 30, 40, and 50% of all days from the time series. As mentioned above, we employ the random walk constraint producing the best overall repeatability (8 mm $\mathrm{hr}^{-1/2}$) and then test how much further the repeatability can be improved by each of the indices.

As mentioned above, the Herstmonceux time series comprises 155 days, 57 of which are affected by fronts. When we set the indices such that exactly 57 days are rejected, we can determine the index performance with respect to its ability to detect frontal days by working out the overlap between the days it rejected and the days affected by fronts. The results are shown in Table 1, which lists the cutoff criteria and overlap with frontal days for each index. For the GRAD index, the closest number of days it was able to reject was 58. In this case, the indicator of tropospheric variability (the number of rapid changes) is an integer. Because some days yielded identical values, only either 58 or 55 days could be excluded but not 57.

The LOC index of tropospheric variability produces the best repeatability in height: The difference in variance between the accepted and rejected days is significant (the reduction of variance is actually greater than when simply eliminating days affected by fronts). After excluding (what it classifies as) the 57 most variable days, the repeatability improves almost from 8 to 7 mm. However the gradient method achieves the highest detection rate of days affected by weather fronts: 40 days out of 57 days were detected (corresponding to 70%). Not all fronts produce rapid changes in delay: We believe that these are the least intense ones where the physical differences between the adjacent air masses are relatively mild (especially occluded fronts). Also, considering that none of the indices

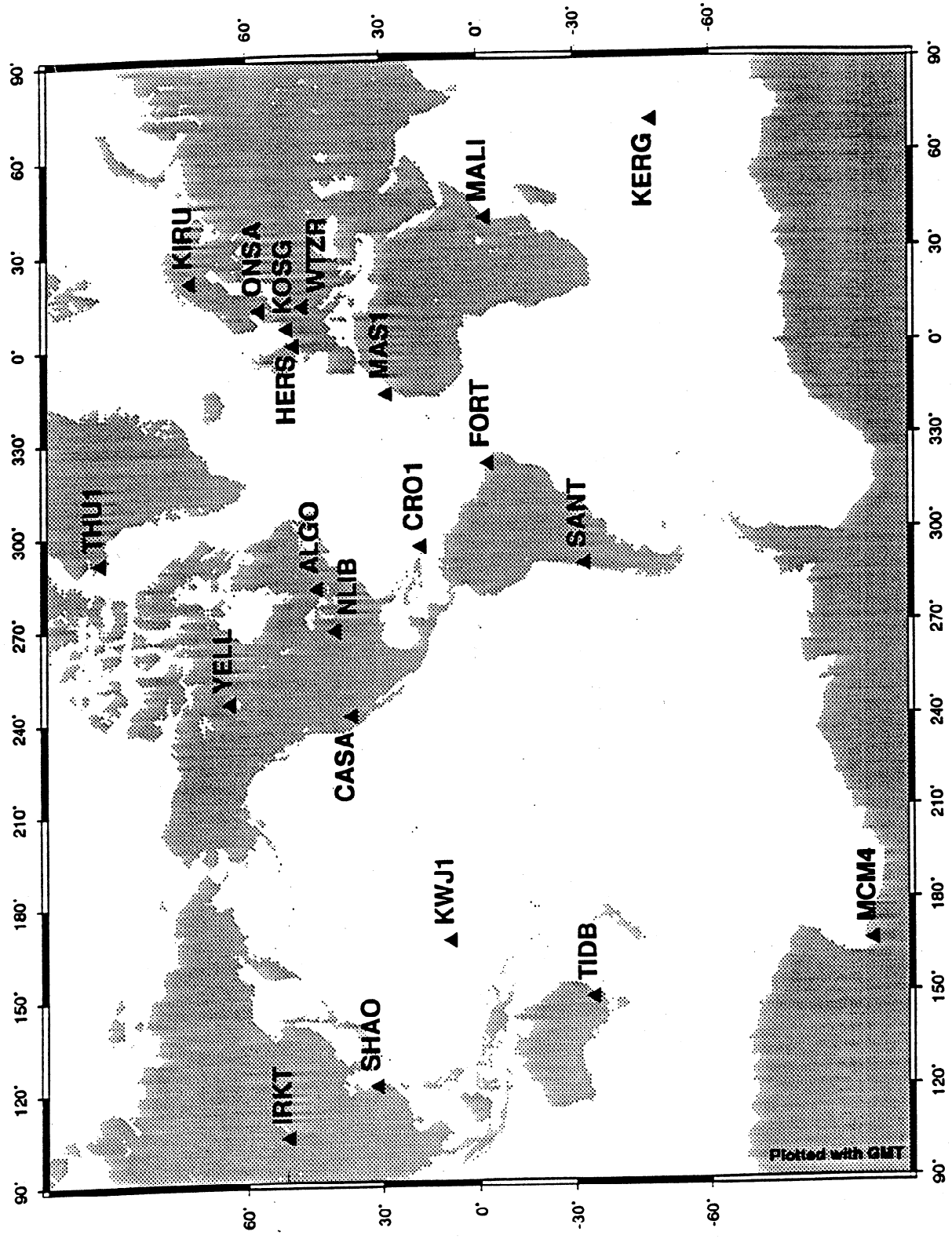
KIRU
ONSA
KOSG
WTZR
HERS
MAS1
MALI
KERG
FORT
THU1
ALGO
NLIB
CRO1
SANT
YELL
CASA
KWJ1
TIDB
MCM4
IRKT
SHAO
Plotted with GMT

Figure 9.

Table 1. Effect of Removing the 57 Most Variable Days Using Tropospheric Indices at Herstmonceux

Index	Index Cutoff	Overlap of Rejected and Frontal Days	Repeatability of the 98 Accepted Days, mm	Resulting Square-Root of Variance Reduction, mm	Repeatability of the 57 Rejected Days, mm	Square-Root of Difference in Variance of the Rejected and Accepted Days, mm
Fronts	n/a	n/a	8.0	2.2	8.4	2.7
FRACT	> 1.0438	54% (31 days)	7.7	2.6	8.8	4.4
LOC	> 31.72	60% (34 days)	7.2	3.8	9.2	5.9
GRAD	> 10	70% (40 days)	7.7	2.6	8.7	4.0

The optimum random walk constraint of 8 mm $hr^{-1/2}$ was applied. Use of troposospheric indices yields greater reductions of variance than eliminating the 57 days affected by weather fronts (denoted as index "fronts"). The overall vertical repeatability, using all 155 days, is 8.1 mm. The 58 most variable days were removed in the case of GRAD.

achieves a detection rate of 100%, there must also occasionally be other phenomena at work that leave a similar signature to weather fronts, although the latter clearly appear to be the main source of disturbance in the tropospheric delay time series.

Since it appears that applying an index can actually be more successful at reducing systematic error than just eliminating days affected by fronts from the time series, another approach to use the indices "blindly" by ignoring the presence of weather fronts altogether and simply trying to improve the repeatability based on the analysis of tropospheric variability only. In this case, however, there is no other option than to choose the cutoff arbitrarily. We therefore test several criteria so that certain percentages of days are rejected (Figure 10). The three indices tested produce comparable results if not more than 20% of the most variable data is excluded from the time series. When removing further days with the (remaining) highest tropospheric variability, the LOC index is the most efficient method at reducing the height scatter: at 40% the repeatability has improved by more than a millimeter (Figure 10).

Another indication of reliability is the vertical station ve-

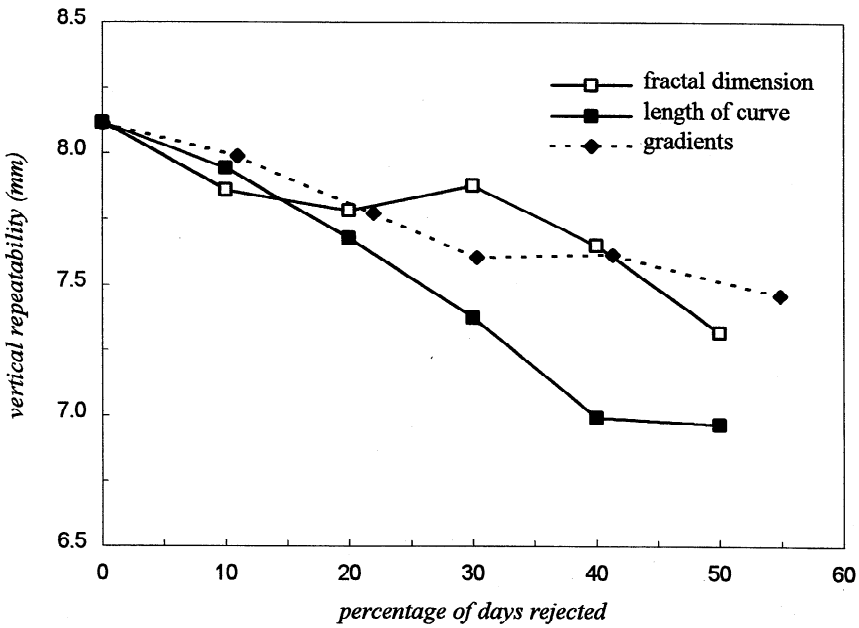

Figure 10. Index performance at Herstmonceux. The repeatability generally improves when removing days with higher tropospheric variability. At the rejection rate of 10%, the fractal dimension is the most efficient index; from 20% onward, the length of curve yields the best repeatabilities.

Figure 9. Global test stations used. They were chosen to cover a wide range of climates: ALGO (Algonquin, Ontario), CASA (Mammoth Lakes, California), CRO1 (St. Croix, Virgin Islands), FORT (Fortaleza, Brazil), HERS (Herstmonceux, England), IRKT (Irkutsk, Siberia), KERG (Port aux Francais, Kerguelen Islands), KIRU (Kiruna, Sweden), KOSG (Kootwijk, The Netherlands), KWJ1 (Kwajalein Atoll, Marshall Islands), MALI (Malindi, Kenya), MAS1 (Maspalomas, Canary Islands), MCM4 (McMurdo, Antarctica), NLIB (North Liberty, Iowa), ONSA (Onsala, Sweden), SANT (Santiago, Chile), SHAO (Sheshan, China), THU1 (Thule, Greenland), TIDB (Tidbinbilla, Australia), WTZR (Wettzell, Germany), and YELL (Yellowknife, Canadian North-Western Territory).

Table 2. Effect of Weather Fronts and Various Indices on Vertical Station Velocity at Herstmonceux

HERS Height Time Series	Vertical Velocity, mm yr^{-1}
Basic (all 155 days)	−3.1
Basic minus 57 days affected by weather fronts	−0.6
Basic minus 57 days with FRACT > 1.0438	+1.8
Basic minus 57 days with LOC > 31.72	+5.5
Basic minus 58 days with GRAD > 10	+2.5

The random walk constraint of 8 mm $hr^{-1/2}$ was applied.

locity, although our data span of only 6 months is rather short for this purpose (so we might reasonably expect errors at the level of several millimeter per year). Herstmonceux, located on southern part of the British mainland, is believed to slowly subside because of relaxation of the peripheral bulge caused by postglacial rebound in the northern part [e.g., *Lambeck and Johnston* 1995]. The rate of this subsidence is probably not more than 1 mm yr^{-1}. Interestingly, after removing the 57 days affected by fronts, the estimated velocity becomes more compliant with the theories of glacial rebound, switching from −3.1 to −0.6 mm yr^{-1} (Table 2). However rejecting the most variable days as detected by each of the three indices produces positive rates. Keeping the short data span in mind, however, these results are for careful consumption only.

4.5. Results at Other Sites

When applying the FRACT, LOC, and GRAD indices to the 20 globally distributed sites listed above, we find that some stations display a significant reduction of systematic error. For this analysis we also use the optimum level of process noise for each station, which we determined by processing the 6-month time series of each site with constraints ranging from 4–14 mm $hr^{-1/2}$, at two-unit step intervals. As shown in Table 3, most stations produced their best repeatability at 6–8 mm $hr^{-1/2}$. Some noisy and humid sites required higher values, whereas stations in dry polar regions required less process noise.

We applied the cutoff criteria determined for Herstmonceux to detect the greatest percentage of weather fronts to the 20 other sites shown in Figure 9 (i.e. >1.0438 for FRACT, >31.72 for LOC, and >10 for GRAD). This way, some stations displayed significant improvements in repeatability but often at a cost of having too much data eliminated (for each index, an average of 8 out of the 20 stations had between 50 and 99% of data rejected this way). However two of the polar sites (MCM4 and THU1) did not have any days eliminated because the troposphere generally lacks rapid tropospheric variations in these regions.

Table 3. Results for the FRACT Index

Station	Optimum Random Walk Constraint, mm $hr^{-1/2}$	Number of Days in Time Series	Vertical Repeatability (All Days), mm	Percentage of Days Rejected	Repeatability of Accepted Days, mm	Repeatability of Rejected Days, mm	Square-Root Difference in Variance (Rejected − Accepted), mm	Square-Root Variance Reduction (All − Accepted), mm
SHAO	12	173	16.8	54.3	14.1	18.3	11.7	9.1
KWJ1	6	182	19.6	56.0	17.9	20.6	10.1	7.9
MALI	8	166	22.5	44.6	21.9	23.3	8.0	5.3
TIDB	10	93	10.8	21.5	9.9	16.0	12.5	4.4
MAS1	14	173	16.8	42.8	16.4	17.6	6.6	4.0
NLIB	8	168	10.5	29.2	9.8	11.9	6.7	3.5
IRKT	6	171	16.0	4.1	15.6	22.7	16.5	3.4
SANT	6	142	11.9	7.0	11.7	15.4	10.1	2.4
HERS	8	155	8.1	19.4	7.8	9.6	5.7	2.3
ALGO	12	183	8.9	30.6	8.7	9.5	3.8	1.7
WTZR	8	176	8.8	8.0	8.6	10.4	5.9	1.5
KIRU	8	178	11.7	5.1	11.7	18.4	14.2	1.3
FORT	6	181	12.5	49.7	12.5	12.6	0.6	0.2
MCM4	4	180	14.7	0.0	14.7	n/a	n/a	0.0
THU1	4	184	12.0	0.0	12.0	n/a	n/a	0.0
YELL	10	180	10.8	11.1	10.8	12.1	5.4	-1.2
CASA	4	175	13.1	8.0	13.1	12.7	-3.2	-1.3
KOSG	12	183	7.6	29.5	7.9	6.7	-4.3	-2.4
ONSA	10	166	7.4	19.3	7.8	5.6	-5.4	-2.4
CRO1	6	158	19.7	18.4	19.9	18.9	-6.1	-2.6

The results use a cut-off of 1.064 as determined at HERS to maximize the number of frontal days in the rejected data (KERG is not included since it suffers from a 99% rejection rate). The sites are sorted in reverse order according to variance reduction (in the last column). TIDB was affected by operational problems which produced two data gaps totaling about 90 days, hence the lower number of data points.

Because many stations had too much data eliminated with the Herstmonceux criteria, we optimized the cutoffs for each index to maximize the number of days affected by fronts among the rejected days, rather than discarding exactly 57 days (using the Herstmonceux data). This was done by a simple algorithm. The days were first sorted in descending order according to tropospheric variability. Before the algorithm was started, a count variable was initialized to zero. Then, scanning the list from top to bottom, if a day was affected by fronts, the count variable was incremented by 1; if it was unaffected, 1 was subtracted from the count. The variability of the day for which the count number was at a peak was then chosen as the rejection threshold (if there was more than one identical peak, the first one down the list was selected). This way, the rejection thresholds for FRACT, LOC and GRAD were 1.0640, 33.00, and 10 (same as above), respectively: for FRACT, 24 out of 30 rejected days were affected by the passage of fronts; for LOC, 27 out of 37 were affected; and for GRAD, 40 out of 58 were affected. Not surprisingly, the improvement of repeatability at Herstmonceux was slightly smaller with these criteria than with those used in Table 1. Because the FRACT and LOC indices now had higher thresholds, they also discarded less days for the 20 global sites. This was especially the case for FRACT, which appeared to be the best index for picking out the worst data while maximizing the number of days being retained in the time series. Although KERG, a particularly variable station, still had 99% of its days rejected, the remaining sites generally had no more than 32% excluded except 5 stations (FORT, MALI, MAS1, KWJ1, and SHAO), which saw between 42 and 56% of their data being rejected (Table 3). With these optimized FRACT criteria, SHAO and TIDB underwent significant reductions of variance; in total, 16 out of the 21 sites had their repeatability improved (including HERS). However 5 stations actually produced worse repeatabilities when applying the FRACT index. These are mostly sites with low repeatability, which is an indication that the tropospheric variability at these stations is not high to begin with, and therefore they might be least expected to benefit from this procedure. As shown in Figure 11, the possible reduction of variance is a largely function of latitude (and therefore, we believe, a function of climate as we will discuss later in this paper).

Weather fronts occur mainly in midlatitudes [e.g. *Barry and Chorley*, 1992], so it is not surprising that it is mostly stations between ~30° and ~55° latitude that benefit from an index. However, some stations less likely to be affected by fronts also had their repeatabilities improved considerably (e.g., MALI and KWJ1). Indices therefore also appear to be useful to reduce systematic error originating from tropospheric variability other than that caused by weather fronts (e.g., as found in humid climates). For each index, we therefore tested fixed rejection rates of 10, 20, 30, 40, and 50% to check the effect of fine-tuning the indices for each site individually, rather than using a universal cutoff. We believe that each station requires individually optimized cutoffs for the indices because tropospheric variability appears to be largely a function of air temperature: The higher the temperature, the more water vapor the air can hold, and the more the humidity can vary. From the 21 sites, 14 have their repeatability improved by 0.3–1.4 mm by at least one of the indices after deleting the 30% most tropospherically variable days in the time series. The most consistent improvement by all three indices was found for Sheshan (SHAO), which is located in a relatively humid climate near Shanghai. Similarly consistent results were obtained at CASA, KWJ1, MALI, and NLIB. For the remaining stations, it was usually the LOC index that produced greater reductions of variance than the other two indices, although the latitude and climate dependence seen in Figure 11 was also visible in the LOC results (using a universal rejection rate of 30%, the correlation between station latitude and index reduction of variance was -0.61). The GRAD index was generally the least efficient with respect to improving the vertical repeatability.

At first sight, one could be tempted to simply explain the fact that some stations benefit more than others from the indices by declaring it consistent with statistical expectation and embark on an elaborate statistical analysis to prove it (e.g., as done by *vanDam et al.* [1994] for their analysis of atmospheric loading effects). Certainly, some sites generally have a higher signal-to-noise ratio than others, which could affect index performance. In this case, however, the type of climate prevailing at the different sites seems to play a crucial role. To prove any correlation between index effectiveness and climate, our sample of 21 stations is too small to infer significant con-

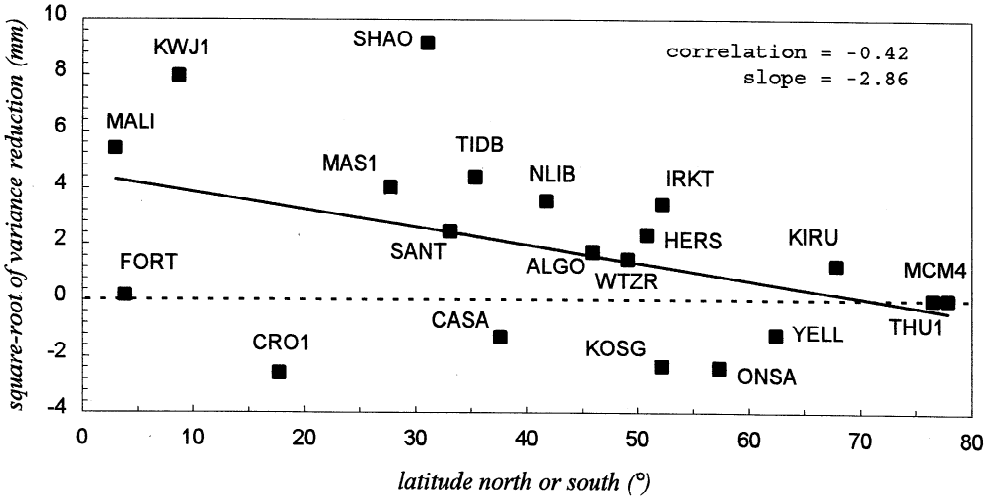

Figure 11. Correlation between the reduction of variance by the FRACT index and the latitude of all sites tested (using the optimized HERS criteria).

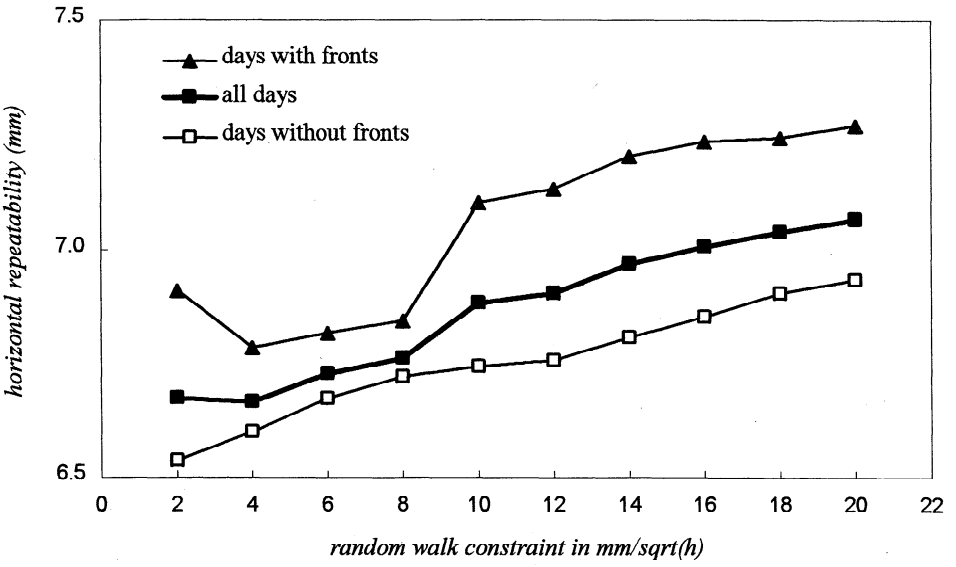

Figure 12. Repeatability as a function of random walk process noise and the passage of weather fronts at HERS for the horizontal station component. Comparing with Figure 8 for the vertical component, the effect is similar but much smaller in magnitude.

clusions. However, we find preliminary indications on the existence of such a correlation, as shown in Figure 11, very encouraging.

4.6. What About the Horizontal Station Component?

So far we have only considered the effect of weather fronts, or indices of tropospheric variability, on station height. However, also the horizontal repeatability is affected, although only by a much smaller magnitude (which is why we have concentrated on the vertical component in this paper). To illustrate this effect, we shall just use Herstmonceux as an example.

Here, weather fronts only contribute $(0.7\ \text{mm})^2$ to the horizontal variance (at 8 mm $\text{hr}^{-1/2}$ process noise), corresponding to 1.1%. The horizontal counterpart to Figure 8, showing the effect of fronts on the repeatability as a function of added process noise, is depicted in Figure 12. At 14 mm $\text{hr}^{-1/2}$, the contribution of fronts to the overall horizontal variance is $(1.5\ \text{mm})^2$, or 4.5%. (Interestingly, it also appears that for the horizontal component it is best to use the smallest possible level of process noise, especially for front-free days.)

In terms of mm^2 of variance, the horizontal contribution of fronts to the full time series is generally ~80% smaller than for the vertical station component. In terms of the contribution of fronts to the variance measured in percent of the variance describing the full time series, the horizontal contribution is ~60% less than the vertical one. The contribution of fronts to the error budget is thus much greater in the vertical than in the horizontal component. We believe that this is due to the very shallow inclination of fronts. Although they are also asymmetric with respect to azimuth, the gradients in horizontal directions are more gradual and spread out than in height, explaining the smaller errors. We therefore also found that tropospheric indices are unable to produce worthwhile improvements in the horizontal component.

5. Discussion

5.1. Sources of Tropospheric Variability

The above analysis concludes that weather fronts have a significant effect on tropospheric delay, which manifests itself in increased systematic error in (especially) height time series. The vertical repeatability of a station can be improved by excluding all days affected by the passage of a front from the series. Similar, if not better, results can be obtained with tropospheric indices. However, because none of these indices achieve a front detection rate of 100%, there also appear to be other phenomena at work that occasionally affect station repeatability in a similar way to weather fronts. It may thus be worthwhile investigating what other sources cause (not necessarily rapid) variations in the estimated residual tropospheric delay. It may not just be of meteorological origin: Signal multipathing or other environment noise could also play a role since the majority of the greatest improvements are obtained at noisy stations (i.e., sites with repeatabilities of, say, 15 mm and above). Higher-order ionospheric effects, which are not eliminated with the ionosphere-free linear combination, may have to be considered as well [e.g. *Bassiri and Hajj*, 1993].

5.2. Correlation Between Daily Residuals and Tropospheric Variability

It is widely accepted that systematic error in the modeled or estimated path delay propagates into a bias in the estimated vertical station component [e.g., *Brunner and Welsch*, 1993]. This is confirmed by our analysis of tropospheric variability. Figure 13 illustrates the relationship between the FRACT index and the height residual for each day at the Sheshan (SHAO) site. The scatter of data points is generally greater on the right-hand side of the plot, i.e., for days with greater fractal dimension and thus increased tropospheric variability. With the optimized Herstmonceux FRACT criterion, the

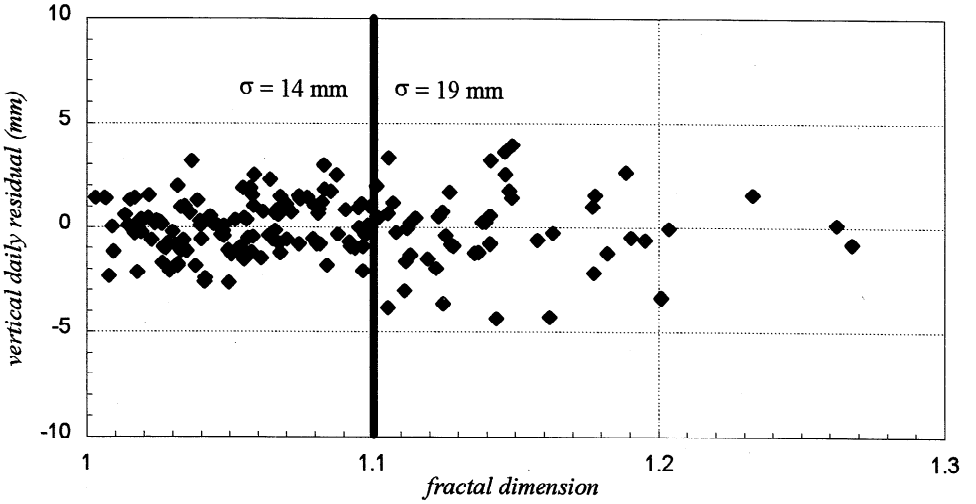

Figure 13. Relationship between daily height residual and tropospheric variability at SHAO. The vertical residuals are determined from a linear regression on the height time series; tropospheric variability is quantified by the FRACT index (see text). The repeatability of the group of days with fractal dimensions of <1.1 is 14 mm; for those with dimensions >1.1, it is 19 mm (the difference is significant).

scatter is divided into two groups containing similar amounts of data: the first group contains the 79 days with tropospheric fractal dimensions of less than 1.0640; The second group includes the 94 days with a fractal dimension greater than that threshold. The difference in repeatability between the first and second group is significant (14.1 versus 18.3 mm). In other words, there is a significant correlation between the variability of the troposphere and the height residual on a particular day. We conclude that conditions of high tropospheric variability are likely to lead to higher systematic errors and therefore higher variability in estimated height. From the plot of Figure 13 it appears that it probably would have been better to apply a less stringent criterion, because the repeatability only starts to get worse beyond a fractal dimension of ~1.1. This highlights the need to customize the indices for each station individually by empirically testing different rejection rates (as described in section 4).

5.3. Effect of Climate and Geographic Site Location

Although our sample of 21 stations is too small to draw significant conclusions on how much the possible reduction of systematic error is a function of site location or climate, the research described in this paper indicates that it is mainly stations in midlatitudes (where weather fronts are most likely to be present), which benefit from the application of tropospheric indices. However the results also suggest that such improvements are not limited to these latitudes only: Some sites located in tropical regions can also have their repeatability enhanced by eliminating the most variable data (e.g., Figure 11). Tropospheric indices are therefore not just useful to detect days affected by fronts from GPS data alone but generally to improve the repeatability of stations that occasionally suffer from rapid tropospheric variations (whatever the cause). The only difficulty is to find the best rejection threshold, since this has to be done empirically. Great care should be taken not to reject too much data because otherwise some of the time series signals may get lost. We believe that most scientists would be reluctant to eliminate >20 or 30% of data from GPS time series. For a fixed rejection threshold of 30%, we found that the LOC index is the most successful at improving repeatability: 10 out of 12 midlatitudinal sites between 30° and 60° thus had their variance reduced by an average of $(6.5\ \text{mm})^2$: ALGO, CASA, HERS, IRKT, KOSG, NLIB, ONSA, SANT, SHAO, and TIDB. Similar improvements for the LOC index are found for the tropical sites FORT, MALI, and KWJ1. The only stations not to benefit from any index (LOC or other) are polar sites. We believe this is due to the fact that the air in polar latitudes is so cold that it cannot hold much moisture, resulting in a stable troposphere and relatively flat curve of tropospheric delay: In general, polar tundras are one of the least stormy areas on Earth [*Hidore and Oliver*, 1993], which explains the inadequacy of our indices here. For example, the curves of tropospheric delay at MCM4 and THU1 were actually so flat that it was not even feasible to determine any gradients steeper than 1 cm hr^{-1}. The situation of the polar sites is further complicated by the fact that these are also expected to suffer additional height variability due to atmospheric loading, which is known to have maximum effect at higher latitudes [*Blewitt et al.*, 1995].

5.4. Occluded Fronts

On a plot of estimated tropospheric delay, it often appears that occluded fronts do not infer as much rapid variation as cold or warm fronts, which is why we did not develop a theoretical model for occlusions. At Herstmonceux, 10 out of the 57 frontal days are affected exclusively by occluded fronts. To the repeatability of the height time series it does not make any difference whether to leave those "occluded" days in or out. However, if we do not classify such days as frontal, the ability of all indices to detect fronts from GPS data alone goes down. As seen above, the FRACT, LOC and GRAD indices are able to detect frontal days with 54, 60, and 70% accuracy, respec-

tively. When we fine-tune these indices to reject 47 days instead of 57, i.e., the number of days affected by cold and warm fronts only, their detection rate goes down to 48, 55, and 62%, respectively. Although occlusions do not seem to be intense enough to insert significant systematic error into a time series, they nevertheless produce enough tropospheric variation to be recognizable by GPS data as a front.

5.5. Implications for GPS Meteorology

We have been able to explain the rapid variations in tropospheric delay caused by the passage of weather fronts with a simple model. We have also apparently been successful in estimating the inclination and passage time of fronts using GPS and a minimal amount of meteorological data input. While it is not surprising that a standard atmospheric model is not appropriate during periods of high tropospheric variability, the front model described in this paper appears to imply that not only the wet but also the dry part of the tropospheric zenith delay deviates from idealized behavior during the passage of fronts. In our example, this becomes especially apparent during the approach of the warm front. Here the standard estimates of the dry delay deviates by up to 2 cm (wet delay, 6 cm) from those computed by our frontal model. *Bevis et al.* [1994] conclude that GPS meteorologists should be able to recover precipitable water (PW) from GPS measurements with an RMS error of <2 mm + 1% of the PW. According to their rule of thumb, stating that the ratio of PW divided by the zenith wet delay equals ~0.15 under average conditions, each centimeter of delay model error would introduce a systematic bias of 1.5 mm to the estimated PW. Current procedures in GPS meteorology derive the wet delay by subtracting the predicted (standard) dry delay from the total delay estimated with GPS. Therefore, the above results suggest that with this approach the estimated PW would be biased by 3 mm during the approach of the warm front, which is outside the acceptable error margin. In regions where fronts are rare, the current procedures to map zenith wet delays onto precipitable water may not be affected, but in the presence of fronts we believe that they could be improved by estimating parameters with a refined version of the front model presented in this paper (ideally it should have some input of radiosonde data to initialize the model with the correct gradients).

Another implication for meteorology is that a single GPS station can be used to monitor the passage and shape of weather fronts. We believe that this could be beneficial for isolated areas, for example, mid-ocean islands, where meteorological data is scarce. In regions where dense GPS meteorology networks exist, we concede that atmospheric scientists would prefer to just feed the GPS estimates of tropospheric zenith delay into their models (rather than secondary products like frontal parameters) because such networks can provide three-dimensional atmospheric tomographies in which frontal structures should easily be recognized. However, remote areas could benefit from the installation of a single GPS receiver, the data of which could then provide the passage times and shape of weather fronts, with possible benefits for climatic research or even operational weather forecasting (particularly now that reasonably precise real-time orbits have become available [see, e.g., *Rocken et al.*, 1997].

Ideally, the frontal parameter estimation should be incorporated in the parameter estimation module of the GPS data reduction software, rather than fitting curves with a multidimensional minimization routine at the end. This would not only streamline the process and ensure that the full information content of the data is exploited, but it could possibly also diminish the need for an a posteriori tropospheric index by reducing systematic error through the additional number of parameters, although this would have to be confirmed by further research.

6. Conclusion

We have shown that the repeatability, or internal precision, of GPS coordinate determinations can be improved especially for midlatitude sites by excluding data acquired during the passage of weather fronts. Alternatively, if no meteorological information is available, a tropospheric index, such as the fractal dimension or length of the tropospheric delay curve, achieves even better results because there also appear to be other phenomena at work that occasionally leave a signature in the tropospheric delay similar to that of a weather front. The highest detection rate of fronts from GPS data alone is achieved with the GRAD index (70%). Fronts affect especially the height of a station and contribute up to 13%, or $(3.2\ \text{mm})^2$, to the vertical variance, depending on the level of process noise applied in the random walk estimation of residual tropospheric zenith delay. Weather fronts also affect the horizontal station component, although only on a much smaller scale which is rather negligible. This might appear to contradict findings of *Rothacher et al.* [1998] who found that tropospheric gradients affect the horizontal more significantly than the vertical. However, there is not a one-to-one correspondence between weather fronts and tropospheric gradients. Future research could focus on synthesizing these two types of investigation. It should be noted that the effect of tropospheric variability (including fronts) on GPS heights becomes more detrimental if a nonoptimum processing strategy is used. At one extreme, if the tropospheric delay is estimated as a constant parameter over successive 24-hour periods, weather fronts contribute 30% to the vertical variance.

There are two implications for GPS meteorology. First, standard atmospheric models are not appropriate to retrieve precipitable water vapor from GPS measurements during periods of frontal influence. Even though this is not a surprising statement, it is interesting to note that our results suggest that also the dry part of the delay significantly deviates from a standard model during the passage of fronts, which would bias the recovery of precipitable water vapor. Second, we have shown that we can estimate the geometry and velocity of a front with a single GPS receiver and minimal input of meteorological data, which we hope could become a new tool for operational weather forecasting or climate analysis of remote regions.

Acknowledgments. The work described in this paper was carried out at the Department of Geomatics, University of Newcastle upon Tyne, England, under contract BFR96/006 with the Luxembourg Government who kindly provided the first author with a substantial research scholarship. We acknowledge financial support from the U.K. Natural Environment Research Council (NERC) under grant number GR3/10041. We thank JPL, California Institute of Technology, for supplying the GIPSY-OASIS II analysis software as well as all required precise orbit and clock solutions, which made precise point positioning possible. We would also like to thank all individuals of the International GPS Service for Geodynamics (IGS) for the free availability of global GPS tracking data, Philip Gibbs at the Royal Greenwich Observatory for providing the HERS met data (funded by

NERC), the U.K. Meteorological Office for full access to their weather chart archives, and Hans van der Marel of Delft University for the Delft GPS and met data. Finally, we would like to thank Mike Bevis, Tonie vanDam, Yoaz Bar-Sever, and Steve Nerem for valuable comments which have improved the quality of this manuscript.

References

Baker, T.F., D.H. Curtis, and A.H. Dodson, Ocean Tide Loading and GPS, *GPS World*, *6*(3), 54–59, 1995.

Barry, R.G., and R.J. Chorley, *Atmosphere, Weather and Climate*, 6th ed, 392 pp., Routledge, New York, 1992.

Bar-Sever, Y.E., P.M. Kroger, and J.A. Boriesson, Estimating horizontal gradients of tropospheric path delay with a single GPS receiver, *J. Geophys. Res.*, *103*, 5019–5035, 1998.

Bassiri, S., and G.A. Hajj, Higher-order ionospheric effects on the Global Positioning System observables and means of modeling them, *Man. Geod.*, *18*, 280–289, 1993.

Bevis M., S. Businger, S. Chiswell, T.A. Herring, R.A. Anthes, C. Rocken, and R. H. Ware, GPS meteorology: Mapping zenith wet delays onto precipitable water, *J. Appl. Meteorol.*, *23*, 379–386, 1994.

Blewitt, G., T. vanDam, and M.B. Heflin, Atmospheric loading effects and GPS time averaged positions, paper presented at *1st Turkish International Symposium on Deformations*, Istanbul, Turkey, Sep. 5 to 9, 1995.

Brunner, F.K., and W.M. Welsch, Effect of the troposphere on GPS measurements, *GPS World*, *4*, 42–51, 1993.

Dixon, T.H., and S.F. Kornreich Wolf, Some tests of wet tropospheric calibration for the CASA UNO Global Positioning System experiment, *Geophys. Res. Lett.*, *17*, 203–206, 1990.

Donn, W.L., *Meteorology*, 518 pp., McGraw-Hill, New York, 1975.

Elgered, G., J.L. Davis, T.A. Herring, and I.I. Shapiro, Geodesy by radio interferometry: Water vapor radiometry for estimation of the wet delay, *J. Geophys. Res.*, *96*, 6541–6554, 1991.

Hidore, J.J., and J.E. Oliver, *Climatology: An Atmospheric Science*, 423 pp., Macmillan, Indianapolis, Indiana, 1993.

Johannson, J.M., A study of precise position measurements using space geodetic systems, *Tech. Rep. No. 229*, School of Elect. and Comput. Eng., Chalmers Univ. of Tech., Göteborg, Sweden, 1992.

Lambeck, K., and P. Johnston, Land subsidence and sea-level change: Contributions from the melting of the last great ice sheets and the isostatic adjustment of the Earth, in *Land Subsidence: Natural Causes, Measurement Techniques, The Groningen Gasfields*, edited by F.G.J. Barends, F.J.J. Brouwer, and F.H. Schröder, 409 pp., A.A. Balkema, Brookfield, Vermont, 1995.

McIntosh, D.H., and A.S. Thom, *Essentials of Meteorology*, 240 pp., Wykeham, London, 1969.

Meteorological Office, *Handbook of Aviation Meteorology*, 3rd ed, 401 pp., Her Majesty's Stationery Office, London, 1994.

Nelder, J.A., and R. Mead, A simple method for function minimization, *Comput. J.*, *7*, 308–313, 1965.

Press, W.H., S.A. Teukolsky, W.T. Vetterling, and B.P. Flanery, *Numerical Recipes in C: The Art of Scientific Computing*, 2nd ed, 994 pp., Cambridge Univ. Press, New York, 1992.

Roach, D.E., and A.D. Fowler, Dimensionality analysis of patterns: Fractal measurements, *Comput. and Geosc.*, *19*, 849-869, 1993.

Rocken, C., T. VanHove, and R. Ware, Near real-time GPS sensing of atmospheric water vapor, *Geophys. Res. Let.*, *24*, 3221–3224, 1997.

Rothacher, M., T. Springer, S. Schaer, and G. Beutler, Processing strategies for regional GPS networks, in *Advances in Positioning and Reference Frames*, vol. 118, edited by F.K. Brunner, 93–100, Springer-Verlag, New York, 1998.

Segall, P., and J.L. Davis, GPS applications for geodynamics and earthquake studies, *Annu. Rev. Earth Plan. Sci.*, *25*, 301–336, 1997.

Smith, E.K., and S. Weintraub, The constants in the equation of atmospheric refractive index at radio frequencies, *Proc. IRE*, *41*, 1035–1057, 1953.

Tralli, D.M., and S.M. Lichten, Stochastic estimation of tropospheric path delays in Global Positioning System geodetic measurements, *Bull. Géod.*, *64*, 127–159, 1990.

van Dam, T.M., G. Blewitt, and M.B. Heflin, Atmospheric pressure loading effects on Global Positioning System coordinate determinations, *J. Geophys. Res.*, *99*, 23,939–23,950, 1994.

Zumberge, J.F., M.B. Heflin, D.C. Jefferson, M.M. Watkins, and F.H. Webb, Precise point positioning for the efficient and robust analysis of GPS data from large networks, *J. Geophys. Res.*, *102*, 5005-5018, 1997.

G. Blewitt, Department of Geomatics, University of Newcastle, Newcastle upon Tyne, NE1 7RU, England. (Geoffrey.Blewitt@ncl.ac.uk)

T. Gregorius, Nederlandse Aardolie Maatschappij B.V., Topographic Section, Postbus 28000, 9400 HH Assen, Netherlands. (T.Gregorius@openmail.xgm-sdm.namass.simis.com)

(Received November 6 1997; revised October 6, 1998;
accepted October 14, 1998)